Journal of Materials Science: Materials in Electronics (2020) 31:8825–8836
https://doi.org/10.1007/s10854-020-03417-4

A one-pot hydrothermal-induced PANI/SnO_2 and PANI/SnO_2/rGO ternary composites for high-performance chemiresistive-based H_2S and NH_3 gas sensors

K. K. Saravanan[1] · P. Siva Karthik[2] · P. Ramnivas Mirtha[3] · J. Balaji[3] · B. Rajeshkanna[1]

Received: 8 November 2019 / Accepted: 13 April 2020 / Published online: 20 April 2020

Abstract
We have fabricated the PANI/SnO_2 and PANI/SnO_2/rGO ternary composites by facile one-step hydrothermal approach followed by polymerization method. The hybrid nanocomposites were scientifically investigated for their structural, morphological and elemental composition through XRD, TEM, EDAX, FTIR and EPR analysis. The tetragonal rutile phase with nanospherical morphology sizes in the range of 25–35 nm was investigated by XRD and TEM results. The N_2 adsorption–desorption measurement showed that ternary PANI/SnO_2/rGO composite showed huge specific surface area (114.51 m^2/g) and pore size (17–21 nm), which is higher than the bare SnO_2 (surface area = 83.51 m^2/g; pore size = 33–37 nm). The chemiresistive-type gas sensor was fabricated and the designed sensors were investigated by their sensing responses towards different gases (ethanol, methanol, carbon monoxide, oxygen, H_2S and NH_3). The results exposed that the ternary PANI/SnO_2/rGO showed high sensing response (56%), fast response (35 s) and recovery time (40 s) towards H_2S gas than other gases. The improved gas-sensing mechanism was also proposed.

1 Introduction

In later times, impressive considerations have been paid by the researchers to manufacture low-cost sensors for detecting harmful and hazardous chemicals or gasses for natural observing [1–5]. For this reason, researchers have as of now examined various nanostructural materials (both inorganic metal oxides and organics) owing to their high surface area, essential for obtaining easy reaction in terms of electrical signals [6]. Due to the increase in factories and vehicles, the natural contamination increments and it seriously harms the environment. Natural contamination includes air pollution, water contamination, soil contamination, etc., which is caused due to the discharge of a few poisonous gas in the air from vehicles, industries and combustion of fossil fuel etc. This air pollutant includes different toxic and hazardous gases such as CO, CO_2, H_2S, Cl_2, and LPG which cause many respiratory diseases [7]. Among them, H_2S is a toxic and harmful gas to human mainly in the workplace that is in risk when there is H_2S gas in the air. Hence, the detection of this harmful gas is very important in our daily life. At present, metal oxide semiconductors (MOS) such as ZnO, SnO_2, WO_3, CuO, In_2O_3 and TiO_2 [8–10] are effectively used as sensing materials for the detection of various harmful and toxic gases, which is present in our environment.

Among the various kinds of MOS, tin oxide (SnO_2) is a wide bandgap (E_g = 3.6 eV, at 300 K) n-type semiconductor and one of the most expansively considered inert oxides for sensing application to sense extensive variety of harmful gases [11–13]. This is due to its high sensitivity, which is harmless, environmental popular and cost effective for making the simple chemical synthesis methods, even though the selectivity and response of different gas towards SnO_2 is low due to the low surface area detection limit. To avoid these drawbacks, combination of binary or ternary component using graphene or polymer-based SnO_2 composite is a new method to improve the sensing response. It is well known that reduced graphene oxide (rGO) and polyaniline (PANI) are novel two-dimensional nanomaterials with

✉ P. Siva Karthik
psivakarthick@yahoo.com

[1] Department of Electrical and Electronics Engineering, University College of Engineering, Thirukkuvalai, Tamilnadu 610 204, India

[2] Department of Chemistry, University College of Engineering, Panruti, Tamilnadu 607 106, India

[3] Department of Physics, University College of Engineering, Panruti, Tamilnadu 607 106, India

effective surface area and high conducting nature which is used to detect various gases [14, 15]. Chu et al. reported the H_2S gas-sensing performance using ternary composite SnO_2–rGO as gas sensor [16]. Cho et al. prepared PSS-doped PANI/graphene composite sensor and detection of H_2S gas with various concentrations at room temperature [17]. Mousavi et al. prepared a flexible gas sensor based on PANI-polyethylene oxide (PEO) and exhibited high response to H_2S gas [18]. The controllable fabrication of highly ordered nanostructure on substrate has been widely studied using different kinds of methods, such as high-temperature vapor-phase approaches including physical vapor deposition and chemical vapor deposition and low-temperature solution-based chemical strategies. Compared with vapor-phase approaches, which are expensive and energy-consuming, solution-based synthetic strategies have the advantages of saving energy, convenient manipulation, excellent control over size and morphology, and greater capability and flexibility. Among them, hydrothermal synthetic strategies on a water system are considered as simple and powerful routes and has become more popular in fabricating ordered nanoarray structures recently. This method relies on the chemical reactions and solubility changes of substances in a sealed heated aqueous solution above ambient temperature and pressure to grow nanocrystals. Hence, we report the high-performance H_2S gas sensor-based PANI/SnO_2/rGO ternary composites as sensing materials, which are synthesized by a facile one-step hydrothermal approach followed by annealing process. The fabricated ternary sensor showed outstanding sensing response, fast response and recovery time as well good selectivity to H_2S gas. To the best of the author's knowledge, this is the first report about chemi-resistive sensor based room temperature high sensing performance of H_2S using PANI/SnO_2/rGO ternary composites as sensing layer.

2 Experimental procedure

2.1 Materials

All reagents used in the experiments such as aniline ($C_6H_5NH_2$), ammonium peroxydisulfate ($(NH_4)_2S_2O_8$), hydrochloric acid (HCl), tin chloride ($SnCl_2$), sodium hydroxide (NaOH), and sulfuric acid (H_2SO_4) were of the analytical grade and used as purchased. Aniline monomer was doubly distilled before use. Double distilled water was used throughout the investigations.

2.2 Synthesis of PANI

PANI was synthesized by the oxidation of aniline with ammonium persulfate. A solution of 0.1 M aniline was prepared using 1 M HCl. A solution of 0.1 M ammonium persulfate was also prepared using distilled water. A known volume of an aniline hydrochloride solution was taken in a 1000 mL beaker and stirred for about 5 min. Then an equivalent quantity of 0.1 M ammonium persulfate was added dropwise and continuously stirred using a magnetic stirrer. After a short time, the reaction took place and PANI was initially formed at the interface of the immiscible solution. The colorless aniline hydrochloride solution slowly turned to green. After an addition of the entire quantity of ammonium persulfate, stirring continued for 15 min. In this way, a dark green colored precipitate of PANI was formed. The precipitate was washed with distilled water several times to remove the impurities. Finally the precipitate was washed with acetone to remove the foreign bodies. Next the precipitate was allowed to dry completely on its own at room temperature. The dried material was stored in an air-tight container. Finally, pure PANI was obtained [19].

2.3 Synthesis of PANI/SnO_2/rGO ternary composite

GO was prepared by Hummers' method [20]. In brief, 2.55 g of $SnCl_2$ (99.99%, Sigma-Aldrich) was dissolved in 50 mL of DI water under continuous magnetic stirring. After dissolving completely, the mixed solution was further nucleated by adding NaOH dropwise until the pH value attains 9. The resultant reaction was transferred to Teflon-lined autoclave maintained at 180 °C for 24 h. Then the clear white color precipitate was cleaned and centrifuges and finally dried at 80 °C for overnight. Then white color SnO_2 nanopowders were obtained. PANI/SnO_2/rGO nanocomposite was synthesized based on the previously reported literature [21–23]. PANI/SnO_2/rGO nanocomposite was synthesized by oxidative interfacial polymerization of aniline in the presence of the as-synthesized SnO_2 nanoparticles using ammonium persulfate (APS) as an oxidant in an acidic medium. Aniline (0.1 M) in 1 M HCl and APS (0.1 M) in chloroform and 0.5 g of prepared GO were dissolved separately and stirred for 1 h. Then an APS-SnO_2-based solution was carefully transferred into an aniline-based solution. The reaction was allowed to proceed for 12 h. At the end of the reaction, a PANI/SnO_2/rGO composite formed was collected by filtration, washed with distilled water and acetone repeatedly until the filtrate was colorless. The collected composite was dried at 80 °C until constant weight was attained.

2.4 Characterization techniques

The Bruker D8 diffractometer has been utilized to analyze the structural properties of the compounds. The morphology and elemental presence was investigated using a JEOL JEM 2100F and A JEOL Model JED-2300. BRUKER RFS 27: spectrometer was used to find out the vibration modes of the

as-obtained samples. Nova 2200e N_2 absorption–desorption was carried out to know the pore distribution and surface area. The thickness of the sensing films was measured by the optical interference method and found to be 2.05 µm.

2.5 Gas sensor setup

A specially designed aluminum cylinder (diameter of 20 cm and length about 40 cm) has been used as the sensor chamber. Sensing film was prepared using the bare and ternary composite nanopowders (10 mg) which were diluted in appropriate amount of water and deposited by drop coating on alumina substrates (5×3 mm^2) on Pt interdigitated electrodes. A DC power supply was produced using 12 V regulated powder supply (Vc) with load resistance of 15 M ohm. A standard millimeter (GDM 8135, China) was used to measure the output voltage (V_{out}) of the sensor. The gases from proficient bottle are introduced through the sensing film by mass flow controller (MFC). The concentration of gas varied from 0 to 100 ppm. The test gas was mixed with dry air to attain the required concentration, and the stream rate was kept up utilizing mass stream controllers. The rotational pump was associated as an outlet to expel the different gasses. The experiment was done at room temperature with 65% of relative humidity. Sensitivity, S, was expressed in terms of sensor resistance in air (R_a) and in test gas (R_g) as follows: $S = R_a/R_g$ [24]. The schematic representation of the fabricated gas sensor device is shown in Fig. 1.

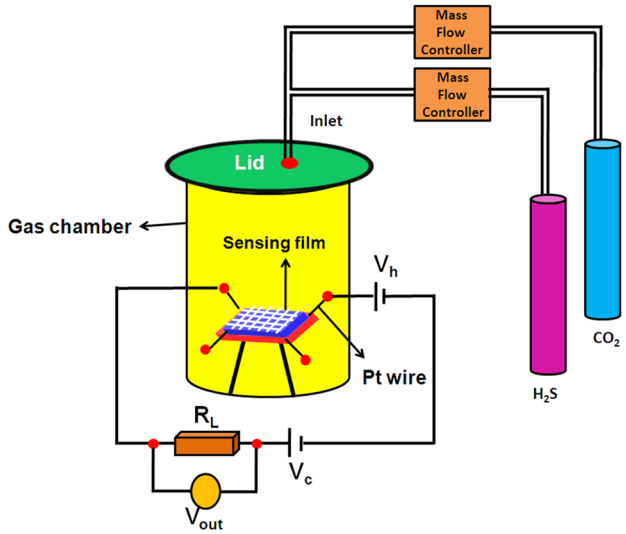

Fig. 1 Schematic representation of the resistive-type gas sensor setup

3 Results and discussion

3.1 XRD analysis

Figure 2a shows the powder XRD pattern of all the obtained sensor samples. In pure PANI sample, three well-known peaks located at $2\theta = 14.9°$, 20.5 ° and 25.8° belongs to the orientation plane of (011), (020) and (200) [25]. Moreover, the pattern of PANI is polycrystalline in nature with broad intensity, which may be due to the reiteration of benzene rings. The peaks positioned at $2\theta = 23.9°$ and 42.3° indicates the rGO plane of (002) and (100), respectively [26]. All the peak positions in the diffraction pattern of bare SnO_2 correspond to tetragonal

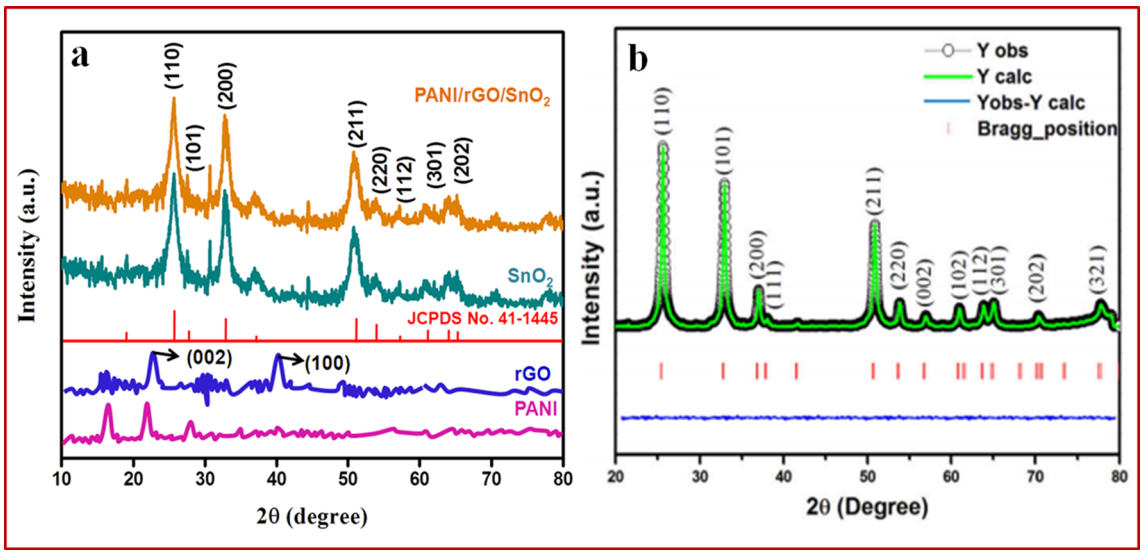

Fig. 2 **a** Powder X-ray diffraction pattern of pure PANI, rGO, SnO_2 and PANI/rGO/SnO_2 composite samples. **b** Rietveld refined XRD spectrum of SnO_2

rutile-type structure with *P42/mnm* symmetry and the results are matched well with the already reported values [27]. The formation all the peaks related to ternary compounds confirms creation of PANI/rGO/SnO_2 ternary compounds. Based on the Scherrer's formula [28], the crystalline size was estimated as 45, 42, 35 and 24 nm for PANI, rGO, SnO_2 and PANI/rGO/SnO_2 composite samples, respectively. The decrease the size of the composite sample is due to the surface modification of SnO_2 due to the decoration of PANI/rGO nanosheets. Compared to the pure SnO_2 sample, intensity of the peak of PANI/SnO_2/rGO composites that became lowering and broadening is observed. This was due to deformation, grain refinement and straining introduced by the carbon and polymer reinforcements. This could be ascribed to two reasons: (1) graphene in the matrix would precipitate at the grain boundaries during solidification and act as a barrier for crystals growth, and (2) graphene/PANI composite can provide more supporting sites for metal nucleation because of their high specific surface area [29, 30]. Figure 2b shows X-ray diffraction pattern with Rietveld refinement of SnO_2. Rietveld refinement of XRD data confirms single-phase of SnO_2 with space group (P42/mnm) and all diffraction peaks are indexed in the tetragonal rutile structure.

3.2 TEM and EDAX analysis

The surface and porosity nature of the products were analyzed through TEM and HRTEM images and is depicted in Fig. 3. Both PANI and rGO showed sheet-like morphology (Fig. 3a, b). However, the bare SnO_2 showed clear spherical-shaped morphology with average diameter of around 32–38 nm (Fig. 3c). Moreover, the spherical nanoparticles are wrapped homogeneously on the sheets in the PANI/rGO/SnO_2 composite (Fig. 3d). In the composite sample, the size of the nanoparticles got reduced to 25–30 nm, which is in good accordance with the crystalline size calculated from the XRD results. In addition, less smoothness and clear pores in the ternary composite can be favorable for developing the gas-sensing nature. The clear lattice fringes of 0.34 nm was observed in the HRTEM image (Fig. 3e) of ternary compound, which is caused by (110) orientation of SnO_2 [31]. The presence of N, C, Sn, and O (Fig. 3f) elements confirms the formation of ternary composite.

3.3 FTIR spectra analysis

The chemical compound and vibration of the functional groups were analyzed using FTIR spectra (Fig. 4). The

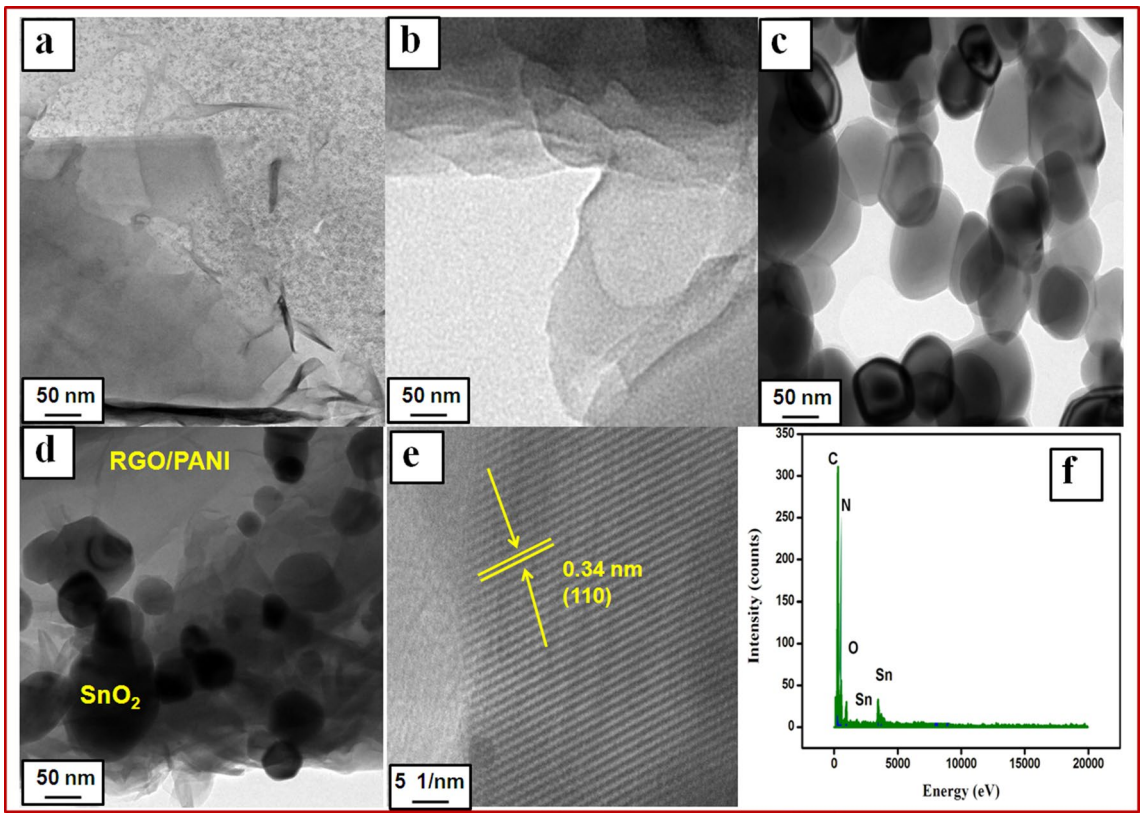

Fig. 3 TEM images of **a** PANI; **b** rGO; **c** SnO_2; **d** PANI/rGO/SnO_2; **e** HRTEM image of PANI/rGO/SnO_2; and **f** EDAX spectra of PANI/rGO/SnO_2

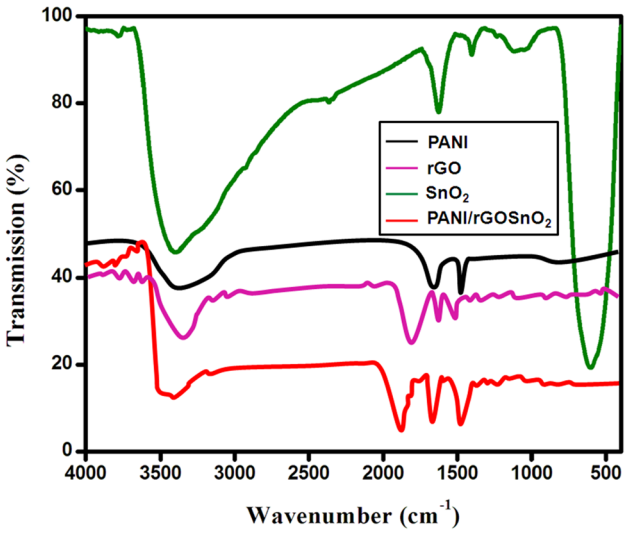

Fig. 4 FTIR spectra of pure PANI, rGO, SnO_2 and PANI/rGO/SnO_2 composite samples

serious of absorption peaks at 3425, 1550 and 1490 cm^{-1} are obtained for bare PANI, which is the characteristic absorption of C–H vibration, C=C and C=N stretching of benzene matrix [32, 33]. C=O in the COOH group vibration for rGO was located at 1748 cm^{-1} [34]. The Sn–O–Sn vibration band of SnO_2 is positioned at 608 cm^{-1} along with surface hydroxyl groups (3435 cm^{-1}) in the bare FTIR spectra proving the formation of SnO_2 nanoparticles [35]. All the relevant vibrations in the composite sample again supported the creation of ternary composite of PANI/rGO/SnO_2.

3.4 UV-DRS analysis

To know the electronic transition and optical bandgap energy of the samples UV-DRS was carried out and the related absorption spectrum is shown in Fig. 5a. From the graph, series of absorption edges were found to be 452, 471, 501 and 523 nm for PANI, RGO, SnO_2, and PANI/RGO/SnO_2 composite samples, respectively. The bandgap energy values linearly decrease for SnO_2 and ternary composite samples. Based on the absorption edges, the calculated bandgap energies are 2.74, 2.62, 2.47 and 2.37 eV, respectively (Fig. 5b). This in turn causes shallow states in the bandgap which has small ionization energies upon increased concentration of guest (PANI and rGO) to the host (SnO_2) material. The added PANI and rGO generates a band. If this band is very close to conduction band or valence band edge, the bandgap value will decrease. The decrease in bandgap energy of the ternary compound is more favorable for improving the gas-sensing performance than bare samples. Because, the electrons are freely trapped from VB to CB of SnO_2 due to the lower bandgap and gas molecules are easily reacted with the free electrons in the surface of sensor, which results in high sensing performance.

3.5 N_2 adsorption–desorption analysis

The textural properties such as pore size and surface area of the samples was analyzed by N_2 adsorption–desorption analysis. Figure 6a and b shows the N_2 adsorption–desorption and corresponding pore seize distribution plot of SnO_2 and PANI/rGO/SnO_2 composite samples, respectively. Type IV isotherm with obvious H3 hysteresis loop was found in both samples, which shows a typical mesoporous nature

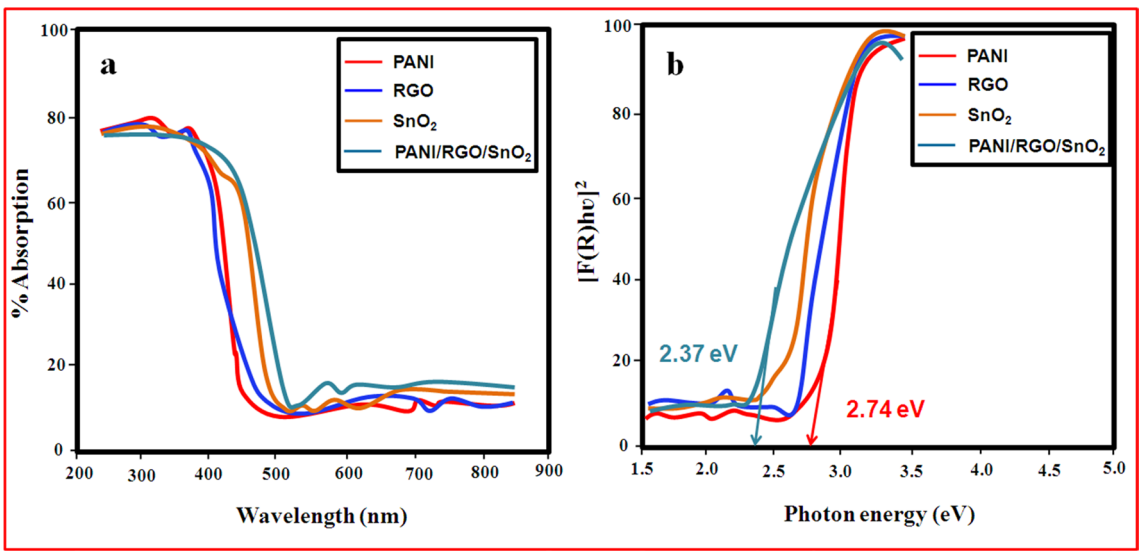

Fig. 5 UV-DRS analysis of PANI, rGO, SnO_2 and PANI/rGO/SnO_2 composite samples. **a** Absorption spectra and **b** K–M model

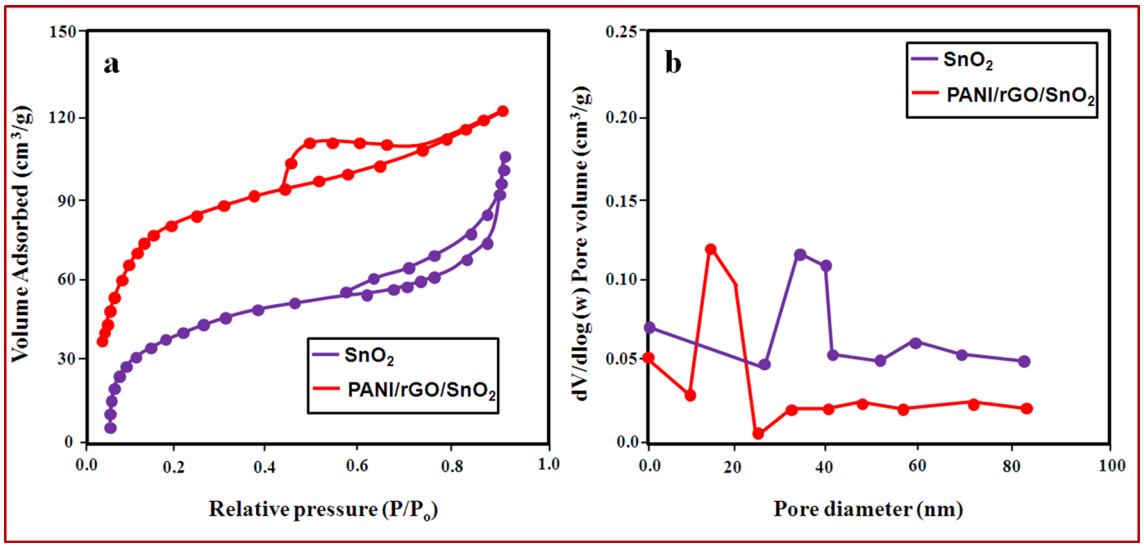

Fig. 6 **a** N_2 adsorption and desorption; **b** pore size distribution of the pure SnO_2 and PANI/rGO/SnO_2 composite samples

of the samples [36–38]. The results express that ternary PANI/SnO_2/rGO composite showed huge specific surface area (114.51 m^2/g) and pore size (17–21 nm), which is higher than the bare SnO_2 (surface area = 83.51 m^2/g; pore size = 33–37 nm). The higher surface nature of the ternary compound is due to the surface interface between the nanosheets (rGO/PANI) and SnO_2 nanoparticles, which is pretty advantageous to the gas-sensing properties.

3.6 Gas-sensing test

The gas-sensing properties of the prepared thick films were tested for H_2S and NH_3 gases with different gas concentrations. The experiment was carried out for RT (27 °C) at the normal atmospheric pressure. The concentration of both gases was varied from 0 to 100 ppm. The spectral response of H_2S and NH_3 gas is plotted in Fig. 7a and b. When the exposure of gas concentration increases (0–100 ppm), the sensing response of both gases were linearly improved. Both gases sensing response denoted that ternary PANI/rGO/SnO_2 showed highest performance such as 56% and 45% for H_2S and NH_3 gas, respectively (at 100 ppm). Moreover, the sensing performance of the all the sensors increases sloppily with respect to gas concentrations. The corresponding graph is shown in Fig. 7c and d. The pretty correlation between the sensor response and the gas concentration is favorable to the practical application of the sensors. Evaluation of response and recovery time of the sensors was significant in the gas-sensing behavior. The response and recovery time was carried out for SnO_2 and PANI/rGO/SnO_2 composite sensor for both gases at concentration of 100 ppm. The consequent graph is shown in Fig. 8a–d. The response and recovery time of H_2S gas is found to be 35 s and 40 s for PANI/rGO/SnO_2 composite sensor, whereas 45 s and 38 s for NH_3 gas, respectively. The result reveals that PANI/rGO/SnO_2 composite sensor showed superior gas-sensing performance than bare sensor. On the whole, gas-sensing parameters are shown in Table 1. The selectivity of the SnO_2 and PANI/rGO/SnO_2 composite sensors were investigated at 100 ppm of different kind of gases such as ethanol, methanol, carbon monoxide, oxygen, H_2S and NH_3 at room temperature. The spectral response is higher for H_2S, which is much better than other gas species (Fig. 9a, b).

Obviously, it is seen that the sensitivity of the sensor to H_2S is 56% which is the maximum response of the four gases. In addition, the sensitivity of the sensor to NH_3 is 381% which is the second maximum response. The sensitivity of the other gases is much lower than the former which is nearly low response. It is revealed that the sensor has more excellent selectivity towards H_2S than ethanol, methanol, carbon monoxide, oxygen, and NH_3. It all comes down to different gases that have different energies when reacting with sensor materials. The reaction of H_2S molecules with the PANI/SnO_2/rGO material could be faster and more responsive. The PANI/SnO_2/rGO sensor is most sensitive to H_2S compared to other gases [39, 40]. Finally, stability test carried out for the sensors were used in the practical point of view. Figure 9c shows the stability test of both sensors towards H_2S gas under same experimental circumstance. The sensor test was tested for 100 days with regular interval for 20 days. After 100 days testing, the sensor retains 95% of origin value (56% of sensing performance). It indicates outstanding stability of the hybrid sensor towards H_2S gas at room temperature. Moreover, the performance of the hybrid sensor obtained in the present work is higher than that of other types of metal oxides obtained in earlier studies

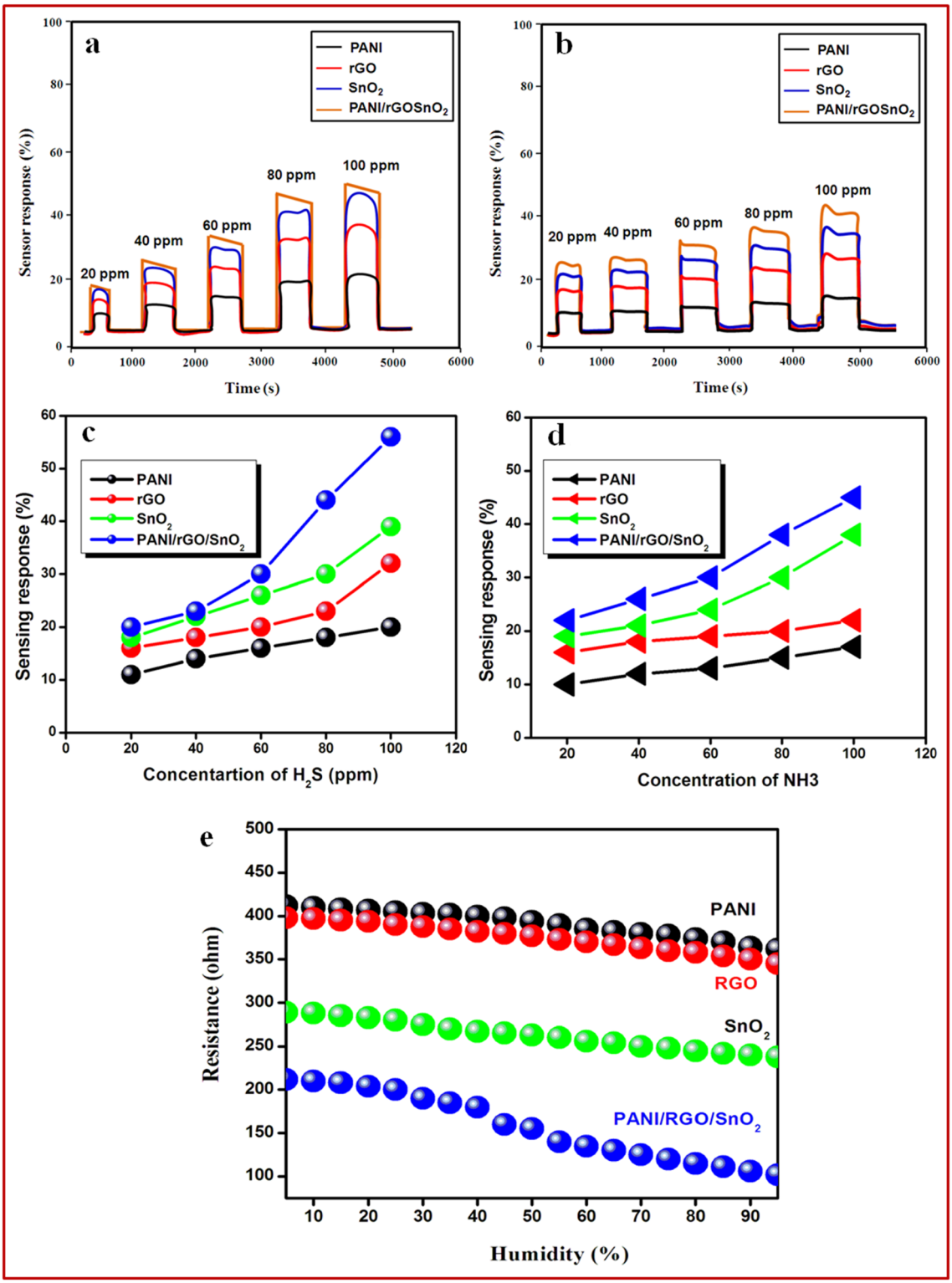

Fig. 7 Spectral response of **a** H_2S and **b** NH_3 gas using different sensors and corresponding sensitivity graph of **c** H_2S and **d** NH_3; **e** effect of humidity on the resistance of the sensor films

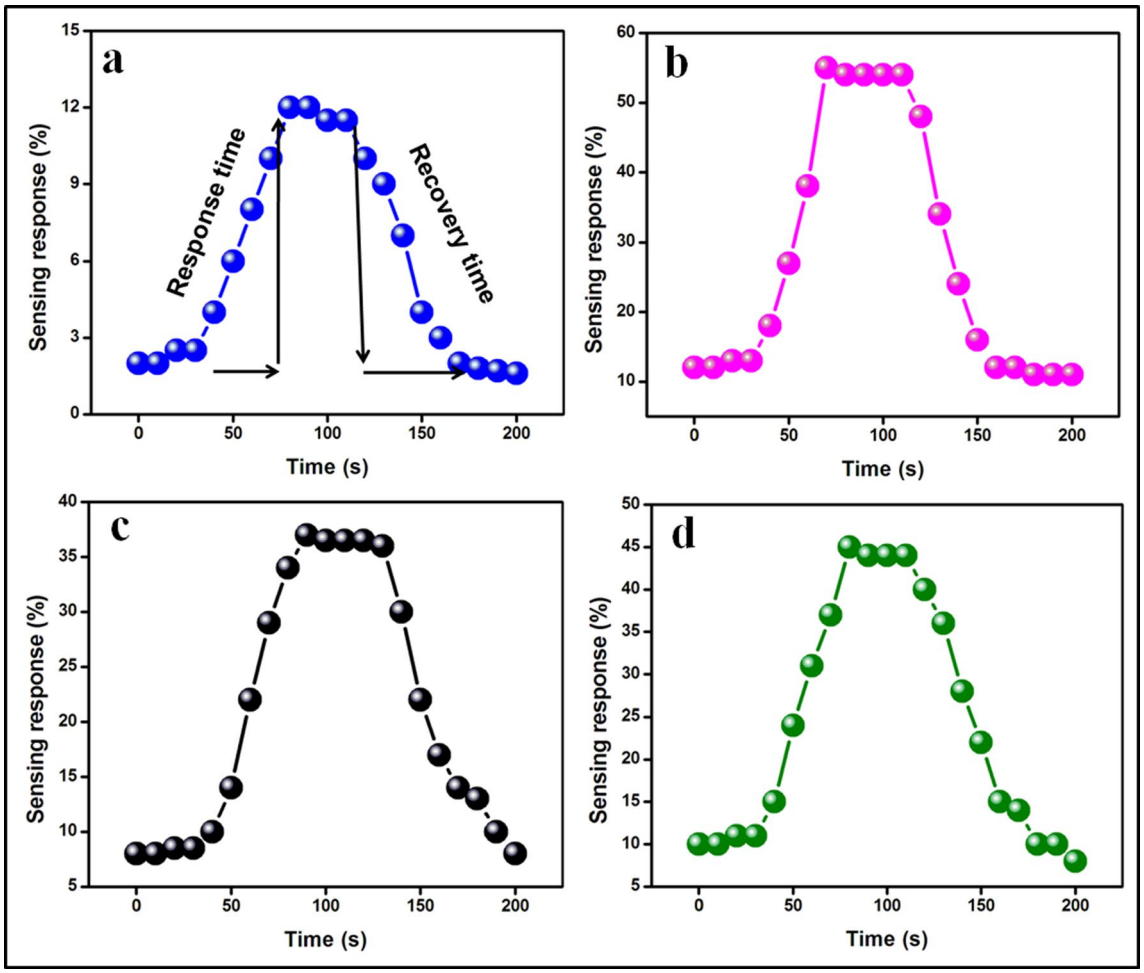

Fig. 8 Response and recovery time of H_2S gas using **a** SnO_2 and **b** PANI/rGO/SnO_2 composite sensors and time response curve of NH_3 gas using **c** SnO_2 and **d** PANI/rGO/SnO_2

Table 1 Gas-sensing parameters of pure PANI, rGO, SnO_2 and PANI/rGO/SnO_2 composite sensors

Samples	Sensitivity (%)		Response time (s)		Recovery time (s)	
	H_2S	NH_3	H_2S	NH_3	H_2S	NH_3
PANI	19	17				
rGO	32	22				
SnO_2	40	38	48	58	50	65
PANI/rGO/SnO_2	56	45	35	40	40	45

[41–45]. The comparison of results of the obtained sensor is also shown in Table 2.

Generally, when the heterojunctions are exposed to the air, oxygen molecules will be adsorbed onto these surfaces,

$$O_2(\text{gas}) \rightarrow O_2(\text{ads}) \quad (1)$$

The O_2 (ads) molecules will capture the free electrons from the conduction band, forming ionized oxygen anions. At room temperature, the ionic O_2^- species are dominant,

$$O_2(\text{ads}) + e^- \rightarrow O_2^-(\text{ads}) \quad (2)$$

contributing to the formation of a low-resistance depletion layer at the sample surface, responsible for an reduces in the overall sample's electrical resistance, which results in high sensitivity. The sensing mechanism of the SnO_2 with presence of oxidization gas and reduction gas are as follows: in the context of REDOX mechanisms, gases such as O_2, NO_2, CO_2, which have the tendency to accept electrons from the metal oxide surface, are termed as oxidizing

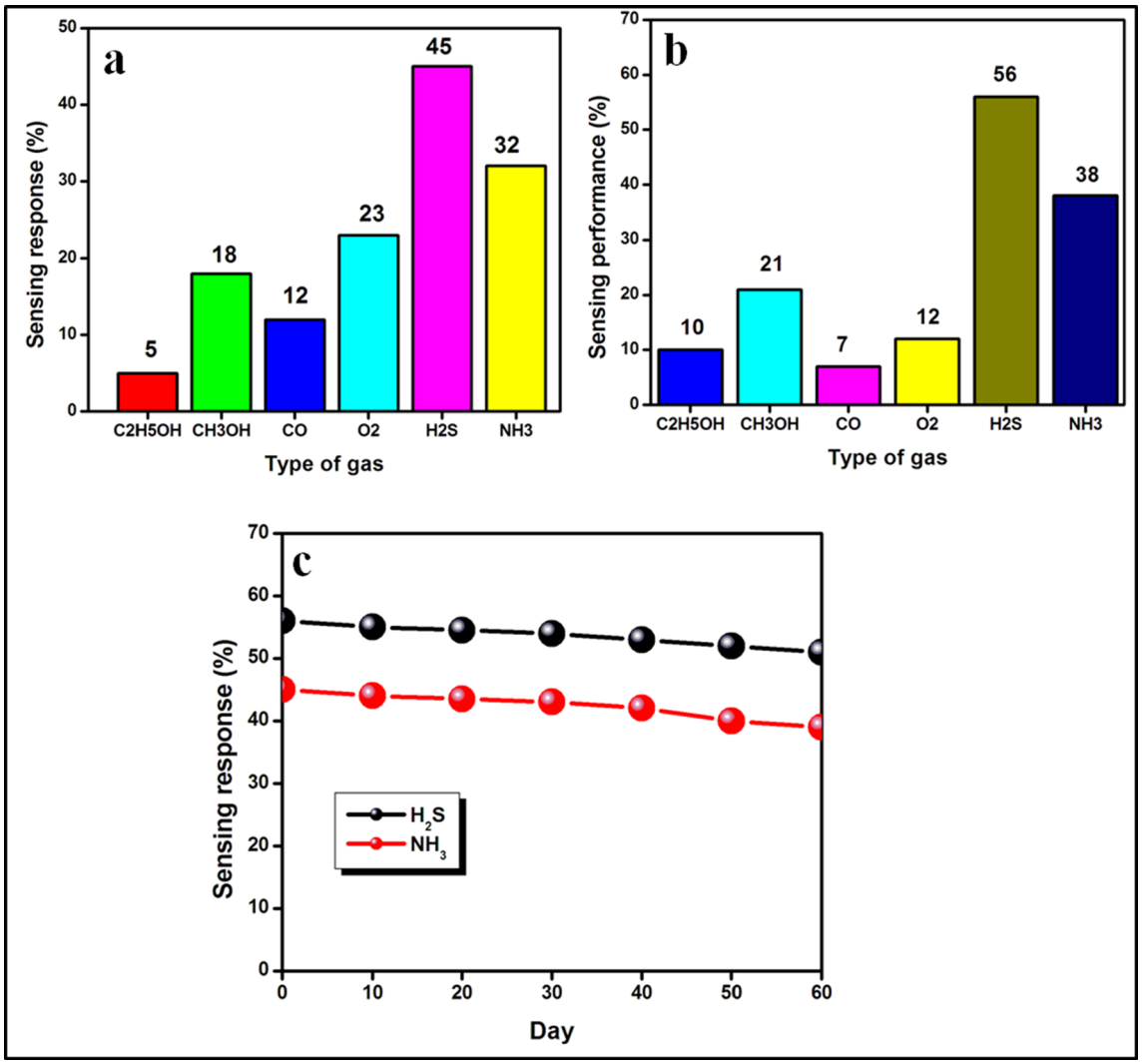

Fig. 9 **a** Selectivity sensing response curve of different gases using **a** SnO_2; **b** PANI/rGO/SnO_2 and **c** stability test of PANI/rGO/SnO_2 composite sensor for H_2S and NH_3 gases, respectively

Table 2 Comparison of H_2S sensing performance between our results and previous works

Materials	Type	ppm level	T°/C	Sensitivity (%)	Reference
SnO_2	Resistive	5	RT	1.45	[34]
SnO_2/rGO	Resistive	5	200	34.0	[35]
SnO_2/rGO	Resistive	100	125	33.2	[36]
Cu_2O-doped SnO_2	Resistive	5	RT	30.0	[37]
Cu_2O-doped SnO_2	Resistive	5	RT	09.0	[38]
Present work	Resistive	10,000	27	52.1	–

gases. Oxygen is the dominant one among oxidizing gases, which adsorbs quickly with metal oxide (SnO_2) surfaces compared to others. The adsorption can be enhanced by increasing the operating temperature, using dopants and by reducing the grain size [46]. But in room temperature (RT), O_2 can accept one electron, and it can accept two electrons from the metal oxide surface (SnO_2) [47, 48]. The adsorbed oxygen molecules/atoms are desorbed quickly, when interacts with other gas molecules. The chemical reaction of O_2 gas with presence of SnO_2 is as follows:

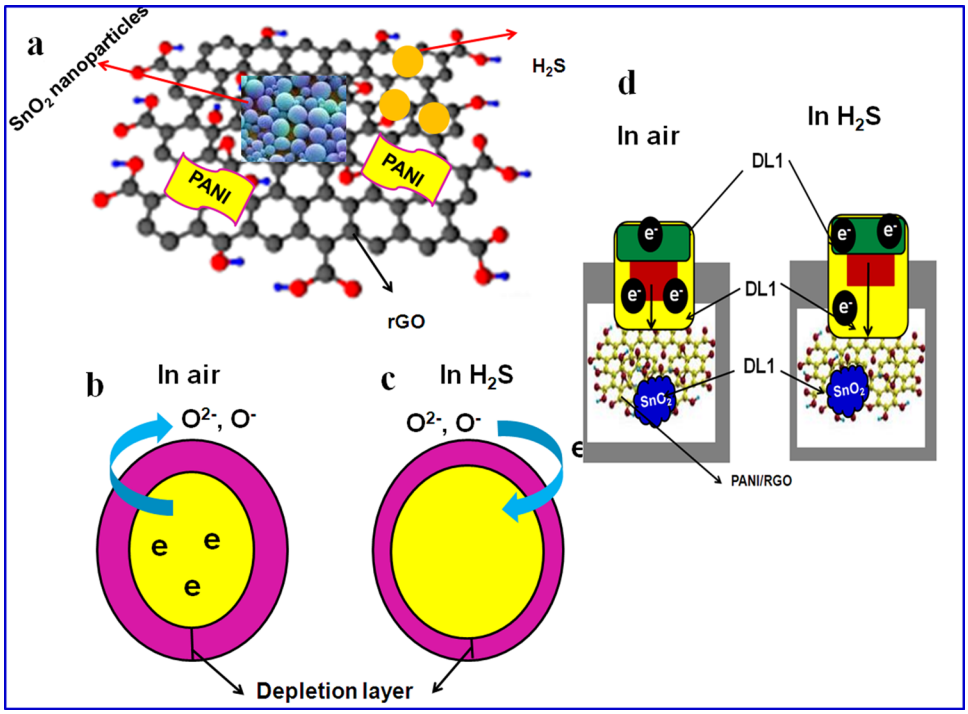

Fig. 10 **a** Mechanism diagram of the SnO2/rGO/PANI; **b** gas-sensing mechanism and electron depletion layer in (**b**) air and **c** H_2S; **d** SnO2/rGO/PANI

$$O_2(\text{gas}) + e^-\left(SnO_2 \text{ surface}\right) \rightarrow O_2^-(\text{adsorbed}) \quad (3)$$

$$O_2^-(\text{adsorbed}) + e^-\left(SnO_2 \text{ surface}\right) \rightarrow 2O^-(\text{adsorbed}) \quad (4)$$

Reducing gases are those which act as electron donors when interacting with metal oxide surface. During this interaction, reducing gases desorb or remove the chemisorbed oxygen ions and physisorbed hydroxyl ions from the metal oxide surface. The variation in the resistance of the material is used to detect the concentration of reducing gases such as SO_2, CO, H_2, NH_3, H_2S and C_2H_5OH by the chemical changes following REDOX reaction. The REDOX equation of H_2S and NH_3 gases is as follows: at low temperature, H_2S directly reacts with lattice oxygen to form SO_4 and produces oxygen vacancy in the surface of the metal oxide which, in turn, increases the conductance as given in Eq. 5:

$$e^-\left(SnO_2 \text{ surface}\right) + H_2S\,(\text{gas}) \rightarrow H_2O + SO_4 + 3V_o^{**} \quad (5)$$

The lone pair of electrons of NH_3 provides strong electron acceptor behavior. But it acts as an electron donor to the metal oxide when reacted with the adsorbed oxygen ions on the surface by reverting the trapped electrons. Free electrons accomplished by the number of oxygen ions reacted with NH_3 molecules, given in Eq. 6

$$e^-\left(SnO_2 \text{ surface}\right) + 2NH_3(\text{gas}) \rightarrow N_2 + 3H_2O + 3e^- \quad (6)$$

The schematic mechanism of the improved sensing performance of PANI/rGO/SnO_2 composite sensor is shown in Fig. 10a. Generally, chemisorbed oxygen ions (O^- or O_2^-) are crucial to interact with the gas molecules on the sensing layer during the chemical reaction. In the ternary compound consisting of SnO_2, spherical is uniformly wrapped on the PANI–rGO sheets. It has high surface area as well as high porous nature than bare SnO_2, which provide large active site to interact the gas on its surface relatively room temperature (Fig. 10a). During the air revelation the thickness of the electron depletion is enhanced on the film surface, which produced high resistance and low sensitivity of the sensing layer (Fig. 10b). With the presence of H_2S gas, the sensor released more number of electrons from its condition band, which results in decreasing the depletion layer as a consequences enhancing the sensing performance (Fig. 10c).

According to our experimental results, PANI/SnO_2–rGO nanocomposites have excellent performance with respect to detection of H_2S, which shows potential for application. The possible sensing mechanism is discussed as follows: as the SnO_2 works as a n-type semiconductor characteristic, when the SnO_2 grain is exposed to the air, the O_2 molecules in air will adsorb on the surface of the SnO_2 grain to form the adsorbed oxygen ions (O_2^-, O^- or O_2^-). As the electrons on the surface of SnO_2 are captured by O_2 molecules, a wide electron depletion layer (DL) is formed. When the SnO_2 which contains adsorbed oxygen ions comes into contact with reducing gases, the trapped electrons will release back to the surface of SnO_2 and the width of the DL will be reduced. SnO_2–rGO nanocomposites possessed n-type

character and electrons acted as electron carriers, and the mechanism is investigated in Fig. 10d. When it is exposed to air, three types of electron DL may be formed, as shown in Fig. 10d. DL1 is the first electron depletion layer, which is formed on the surface of SnO_2 nanoparticles owing to the adsorbed oxygen ions; DL2 is the second electron depletion layer, which is formed by the electrons and transfers from the surface of SnO_2 to the rGO during the formation of p–n heterojunctions; and DL_3 is the third electron depletion layer. It appears in the area where SnO_2 is embedding in rGO nanosheets and forms the p–n heterojunctions. All these electron depletion layers will prevent the migration of electron, leading to the high-resistance state of the nanocomposites. When the reducing gas is introduced, the width of these three types DLs will undergo different changes. The trapped electrons in the DL1 will be released back to the SnO_2, decreasing the width of the DL1; generally, DL2 is supposed to be decreased because the reducing gas molecules may be adsorbed on the surface of rGO and donate the electrons to it, which results in enhanced sensing performance (Fig. 10).

4 Conclusion

This study fabricates the ternary composite sensor of PANI/rGO/SnO_2 nanocomposites using aqueous solution by facile hydrothermal route followed by polymerization process. The as-synthesized sensors were investigated through different studies such as XRD, TEM, EDS, FTIR and BET analysis. The chemiresistive-type gas sensor was fabricated and the designed sensors were investigated for their sensing responses towards different gases (ethanol, methanol, carbon monoxide, oxygen, H_2S and NH_3). The results exposed that the ternary PANI/SnO_2/rGO showed high sensing response (56%), fast response (35 s) and recovery time (40 s) towards H_2S gas than other gases. This work confirmed that the PANI/rGO/SnO_2 ternary sensor is a good candidate for the detection of H_2S gas at RT. The significant enhancement in the gas-sensing performance of the ternary composite is due to the introduction and wrapping of GO and PANI on spherical SnO_2. Hence, the ternary composite show larger BET surface area and smaller mesoporous channels can effectively promote diffusion and adsorption of gas molecules, improving gas-sensing performance of gas sensors.

References

1. A. Kaushik, R. Kumar, S.K. Arya, M. Nair, B.D. Malhotra, S. Bhansali, Organic-inorganic hybrid nanocomposite-based gas sensors for environmental monitoring. Chem. Rev. **115**, 4571–4606 (2015)
2. X. Li, C. Wang, H. Guo, P. Sun, F. Liu, X. Liang, G. Lu, Double-shell architectures of $ZnFe_2O_4$ nanosheets on ZnO hollow spheres for high-performance gas sensors. ACS Appl. Mater. Interfaces **7**, 17811–17818 (2015)
3. T. Jiang, Z. Wang, Z. Li, W. Wang, X. Xu, X. Liu, J. Wang, C. Wang, Synergic effect within n-type inorganice p-type organic nano-hybrids in gas sensors. J. Mater. Chem. C **1**, 3017–3025 (2013)
4. S. Chen, G. Sun, High sensitivity ammonia sensor using a hierarchical polyaniline-/poly (ethylene-co-glycidyl methacrylate) nanofibrous composite membrane. ACS Appl. Mater. Interfaces **5**, 6473–6477 (2013)
5. H.-J. Kim, H.-M. Jeong, T.-H. Kim, J.-H. Chung, Y.C. Kang, J.-H. Lee, Enhanced ethanol sensing characteristics of In_2O_3 decorated NiO hollow nanostructures via modulation of hole accumulation layers. ACS Appl. Mater. Interfaces **6**, 18197–18204 (2014)
6. S. Park, S. Kim, G.-J. Sun, C. Lee, Synthesis, structure, and ethanol gas sensing properties of In_2O_3 nanorods decorated Bi_2O_3 nanoparticles. CS Appl. Mater. Interfaces **15**, 8138–8146 (2015)
7. M. Poloju, N. Jayababu, M.V.R. Reddy, mproved gas sensing performance of Al doped ZnO/CuO nanocomposite based ammonia gas sensor. Mater. Sci. Eng. B. **227**, 61–67 (2018)
8. T. Gao, T.H. Wang, Synthesis and properties of multipod-shaped ZnO nanorods for gas-sensor applications. App. Phys. A **80**, 1451–1454 (2005)
9. J.L.K. Jayasingha, K.M. Jayathilaka, M.S. Gunewardene, D.P. Dissanayake, J.K. Jayanetti, Electrodeposited n-type cuprous oxide cubic nanostructures for liquefied petroleum gas sensing. Phys. State Solid **8**, 1–8 (2016)
10. M. Parthibavarman, B. Renganathan, D. Sastikumar, Development of high sensitivity ethanol gas sensor based on Co-doped SnO_2 nanoparticles by microwave irradiation technique. Curr. Appl. Phys. **13**, 1537–1544 (2013)
11. W. G€opel, K.D. Schierbaum, SnO_2 sensors-current status and future prospects. Sens. Actuators B Chem. **26**, 1–12 (1995)
12. S. Kanan, O. El-Kadri, A. Abu-Yousef, M. Kanan, Semiconducting metal oxide based sensors for selective gas pollutant detection. Sensors **9**, 8158–8196 (2009)
13. S. Liu, L. Li, W. Jiang, C. Liu, W. Ding, W. Chai, Crystallinity and morphology controlled synthesis of SnO_2 nanoparticles for higher gas sensitivity. Power Technol. **245**, 168–173 (2013)
14. H. Khan, K. Malook, M. Shah, Highly selective and sensitive ammonia sensor using polypyrrole/V_2O_5 composites. J. Mater. Sci. **28**, 13873–13879 (2017)
15. D. Zhang, Z. Wu, X. Zong, Metal-organic frameworks-derived zinc oxide nanopolyhedra/S, N: graphene quantum dots/polyaniline ternary nanohybrid for high-performance acetone sensing. Sens. Actuators B **288**, 232–242 (2019)
16. J. Chu, X. Wang, D. Wang, A. Yang, P. Lv, Y. Wu, M. Rong, L. Gao, Highly selective detection of sulfur hexafluoride decomposition components H_2S and SOF_2 employing sensors based on tin oxide modified reduced graphene oxide. Carbon **135**, 95–103 (2018)
17. S. Cho, J. Lee, J. Jun, S. Kim, J. Jang, Fabrication of water-dispersible and highly conductive PSS-doped PANI/graphene nanocomposites using a high-molecular weight PSS dopant and their application in H_2S detection. Nanoscale **6**, 15181–15195 (2014)
18. S. Mousavi, K. Kang, J. Park, I. Park, A room temperature hydrogen sulfide gas sensor based on electrospun polyaniline–polyethylene oxide nanofibers directly written on flexible substrates. RSC Adv. **6**, 104131–104138 (2016)
19. A. Abdolahi, E. Hamzah, Z. Ibrahim, S. Hashim, Synthesis of uniform polyaniline nanofibers through interfacial polymerization. Materials **5**, 1487–1494 (2012)
20. W.S. Hummers, R.E. Offeman, Preparation of graphitic oxide. J. Am. Chem. Soc. **80**, 1339–1339 (1958)

21. D.R. Bijwe, S.S. Yawale, S.P. Yawale, Synthesis of nano (PANI–SnO_2) composites and study of D.C. conductivity. Sci. Rev. Chem. Commun. **2**(2012), 368–371 (2012)
22. B.P. Prasanna, D.N. Avadhani, V. Raj, K. YogeshKumar, M.S. Raghu, Fabrication of PANI/SnO_2 hybrid nanocomposites via interfacial polymerization for high performance supercapacitors applications. Surf. Eng. Appl. Electrochem. **55**, 463–471 (2019)
23. V.S. Reddy Channu, R. Holze, Synthesis and characterization of a polyaniline-modified SnO_2 nanocomposite. Ionics **18**, 495–500 (2012)
24. P. Chaudhari, S. Mishra, Effect of CuO as a dopant in TiO_2 on ammonia and hydrogen sulphide sensing at room temperature. Measurement **90**, 468–474 (2016)
25. S. Liu, Z. Wang, Y. Zhang, C. Zhang, T. Zhang, High performance room temperature NO_2 sensors based on reduced graphene oxide-multiwalled carbon nanotubes-tin oxide nanoparticles hybrids. Sens. Actuators B **211**, 318–324 (2015)
26. Z.Y. Sui, Y.N. Meng, P.W. Xiao, Z.Q. Zhao, Z.X. Wei, B.H. Han, Nitrogen doped graphene aerogels as efficient supercapacitor electrodes and gas adsorbents. ACS Appl. Mater. Interfaces **7**, 1431–1438 (2015)
27. M. Parthibavarman, S. Sathishkumar, M. Jayashree, R. BoopathiRaja, Microwave assisted synthesis of pure and Ag doped SnO_2 quantum dots as novel platform for high photocatalytic activity performance. J. Cluster. Sci. **30**, 351–363 (2019)
28. M. Parthibavarman, K. Vallalperuman, S. Sathishkumar, M. Durairaj, K. Thavamani, A novel microwave synthesis of nanocrystalline SnO_2 and its structural optical and dielectric properties. J. Mater. Sci. Mater. Electron. **25**(9), 730–735 (2014)
29. H. Seema, K. Christian Kemp, V. Chandra, K.S. Kim, Graphene-SnO_2 composites for highly efficient photocatalytic degradation of methylene blue under sunlight. Nanotechnology **23**, 355705 (2012)
30. Z. Du, X. Yin, M. Zhang, Q. Hao, Y. Wang, T. Wang, In situ synthesis of SnO_2/graphene nanocomposite and their application as anode material for lithium ion battery. Mater. Lett. **64**, 2076–2079 (2010)
31. C. Zhang, Y. Cao, P. Li, J. Wu, X. Zong, Humidity-sensing performance of layer-by-layer self-assembled tungsten disulfide/tin dioxide nanocomposite. Sens. Actuators B **265**, 529–538 (2018)
32. X. Lu, Y. Hu, W. Li, Q. Guo, S. Chen, S. Chen, H. Hou, Y. Song, Macroporous carbon/nitrogen-doped carbon nanotubes/polyaniline nanocomposites and their application in supercapacitors. Electrochim. Acta **189**, 158–165 (2016)
33. R. Oraon, A. De Adhikari, S.K. Tiwari, G.C. Nayak, Nanoclay based graphene polyaniline hybrid nanocomposites: promising electrode materials for supercapacitors. RSC Adv. **5**, 68334–68344 (2015)
34. W.S. Wang, D.H. Wang, W.G. Qu, L.Q. Lu, A.W. Xu, Large ultrathin anatase TiO_2 nanosheets with exposed 001 facets on graphene for enhanced visible light photocatalytic activity. J. Phys. Chem. C **116**, 19893–19901 (2012)
35. S. Sarkar, R. Borah, A.L. Santhosha, R. Dhanya, C. Narayana, A.J. Bhattacharyya, S.C. Peter, Heterostructure composites of rGO/GeO_2/PANI with enhanced performance for Li ion battery anode material. J. Power Sources **306**, 791–800 (2016)
36. R. BoopathiRaja, M. Parthibavarman, Hetero-structure arrays of $MnCo_2O_4$ nanoflakes@ nanowires grown on Ni foam: design, fabrication and applications in electrochemical energy storage. J. Alloy. Compd. **811**, 152084 (2019)
37. R. Boopathi Raja, M. Parthibavarman, A. Nishara Begum, Hydrothermal induced novel $CuCo_2O_4$ electrode for high performance supercapacitor applications. Vacuum **165**, 96–104 (2019)
38. Y. Chen, S.H. Lv, C.L. Chen, C.J. Qiu, X.F. Fan, Z.C. Wang, Controllable synthesis of Ceria nanoparticles with uniform reactive 100 exposure Planes. J. Phys. Chem. C. **118**, 4437–4443 (2014)
39. Y. Zhao, J. Zhang, Y. Wang, Z. Chen, A highly sensitive and room temperature CNTs/SnO_2/CuO sensor for H_2S gas sensing applications. Nanoscale Res. Lett. **15**, 40 (2020)
40. L.A. Patil, D.R. Patil, Heterocontact type CuO-modified SnO_2 sensor for the detection of a ppm level H_2S gas at room temperature. Sens. Actuator B. **120**, 316–323 (2006)
41. J. Tian, F. Pan, R. Xue, W. Zhang, X. Fang, Q. Liu, Y. Wang, Z. Zhang, D.A. Zhang, Highly sensitive room temperature H_2S gas sensor based on SnO_2 multi-tube arrays bio-templated from insect bristles. Dalton Trans. **44**, 7911–7916 (2015)
42. S. Choi, B. Jang, S. Lee, B.K. Min, A. Rothschild, I. Kim, Selective detection of acetone and hydrogen sulfide for the diagnosis of diabetes and halitosis using SnO_2 nanofibers functionalized with reduced graphene oxide nanosheets. ACS Appl. Mater. Interface. **6**, 2588–2597 (2014)
43. J. Wang, X. Li, Y. Xia, S. Komarneni, H. Chen, J. Xu, L. Xiang, D. Xie, Hierarchical ZnO nanosheet-nanorod architectures for fabrication of poly(3-hexylthiophene)/ZnO hybrid NO_2 sensor. ACS Appl. Mater. Interfaces **8**, 8600–8607 (2016)
44. N.S.A. Eoma, H.-B. Chob, Y. Song, G.M. Go, J. Lee, Y. Choa, Room-temperature H_2S gas sensing by selectively synthesized Cu_x(x=1,2)O:SnO_2 thin film nanocomposites with oblique & vertically assembled SnO_2 ceramic nanorods. Sens. Actuators B Chem. **273**, 1054–1061 (2018)
45. J. Shu, Z. Qiu, S. Lv, K. Zhang, D. Tang, Cu^{2+}-doped SnO_2 nanograin/poly pyrrole nanospheres with synergic enhanced properties for ultrasensitive room-temperature H_2S gas sensing. Anal. Chem. **89**, 11135–11142 (2017)
46. N. Yamazoe, New approaches for improving semiconductor gas sensors. Sens. Actuat. B **5**, 7–19 (1991)
47. N. Yamazoe, G. Sakai, K. Shimanoe, Oxide semiconductor gas sensors. Catal. Surv. Asia **7**, 63–75 (2003)
48. S. Capone, P. Siciliano, Gas sensors from nanostructured metal oxides. Encycl. Nanosci. Nanotechnol. **3**, 769–804 (2004)